buildings

MDPI

Article

The Influence of Box-Strengthened Panel Zone on Steel Frame Seismic Performance

Linfeng Lu *, Jichen Zhang, Gaowei Zhang, Hao Peng, Bingyou Liu and Hanlin Hao

School of Civil Engineering, Chang'an University, 75 Chang'an Middle Rd, Xi'an 710062, China; 2023228008@chd.edu.cn (J.Z.); 2023228047@chd.edu.cn (G.Z.); 2023228056@chd.edu.cn (H.P.); 2023228019@chd.edu.cn (B.L.); 2021128031@chd.edu.cn (H.H.)
* Correspondence: lulinfeng@chd.edu.cn

Abstract: During the Northridge earthquake, extensive brittle failures on the weld zones of the beam bottom flanges in the rigidity connection of steel special moment frames (SMFs) were detected. One of the primary reasons is the high-tensile strain demand created at the beam bottom flange zones due to positive bending. The weak panel zone of the I-section column exhibits more shear deformation, which promotes and accelerates the brittle fracture of the beam bottom flange weld zones. A box-strengthened panel zone can minimize the shear deformation of the panel zone of the I-section column, which may also reduce the inter-story displacement of steel SMFs and enhance their seismic behavior. In order to investigate this fact, in this research we carried out a model test of a steel frame with a box-strengthened panel zone to examine SMFs' seismic performance and inter-story displacement, as well as testing the contribution of panel zone shear deformation to inter-story drift. Numerical methods were then used to investigate the influence of the axial compression ratio and beam-to-column linear stiffness ratio on the effect of shear deformation on the box-strengthened panel zone. Design recommendations are given based on the research results.

Keywords: steel frame; seismic performance; panel zone; shear deformation; story drift

check for updates

Citation: Lu, L.; Zhang, J.; Zhang, G.; Peng, H.; Liu, B.; Hao, H. The Influence of Box-Strengthened Panel Zone on Steel Frame Seismic Performance. *Buildings* **2023**, *13*, 3042. https://doi.org/10.3390/buildings13123042

Academic Editor: Hiroshi Tagawa

Received: 9 November 2023
Revised: 3 December 2023
Accepted: 5 December 2023
Published: 7 December 2023

1. Introduction

The 1994 Northridge earthquake in California significantly impacted seismic steel research, design, and construction practices, particularly concerning steel special moment frames (SMFs) and their performance during earthquakes, which has raised concerns regarding the reliability of the pre-Northridge connection method and prompted engineers to rethink the design of connections and construction details of connections in steel moment frames. However, all of the various types of connections are based on two concepts: (i) strengthening the connection and (ii) weakening the beam ends. The overall goal in developing new connections is to provide a highly ductile response, reliable performance, and economy.

Before the Northridge earthquake, steel SMFs were widely considered one of the most effective systems for earthquake resistance. These frames were designed to produce ductile responses during earthquakes. This ductile behavior was expected to occur through flexural hinges at the beam-to-column connections and shear yielding in the column panel zone, resulting in a ductile plastic mechanism in the frame. However, many multi-story steel structures with SMFs during the earthquake had brittle fractures in the beam-to-column moment connections [1–5]. These incidents generated severe concerns about the design and construction of SMFs, resulting in a design revolution in steel frame joints and connections. Steel frame connections have since been classified as pre- and post-Northridge connections.

Researchers conducted tests and other investigations to determine the causes of the failure of the pre-Northridge connections and constructed several post-Northridge connections to prevent brittle earthquake failure [5]. Koetaka et al. [6] proposed a novel weak-axis column bending connection with hysteretic dampers. Their test demonstrated that the proposed connection achieved stable hysteretic performance in an extensive deformation range because yielding was limited only in the dampers. Cabrero and Bayo [7,8] performed an experimental and a theoretical study to investigate the behavior of extended end-plate connections in both major and minor column axes subjected to a three-dimensional loading. The tested minor-axis joints consisted of two partial end plates outside welded to the column flange. Similarly, Kim et al. [9] proposed three new weak-axis connection types with welded split and end plates. They reported that these types were easy to construct and ensured the flexural behavior of weak-axis moment connections. This weak axis connection was tested and reported again by Lee et al. [10]. Lee et al. [11,12] investigated the seismic performance of six types of weak-axis column-tree connections through cyclic testing of six full-scale specimens. The effects of beam splice length on the seismic performance of weak-axis column-tree connections were experimentally investigated. Additional work has been conducted by Shim et al. [13]. They proposed a weak-axis system, which mainly used bolts, as shown in Figure 1. In their research, eight interior joint specimens were tested to verify the structural behavior of the proposed connection, and their test results demonstrated that it behaved better than the standard weak-axis connection and had excellent constructability. Kozlowski [14] presented a comprehensive analytical model to predict the moment resistance, initial stiffness, and rotation capacity of semi-rigid weak axis composite connections, and comparative analysis with test results showed a good correlation.

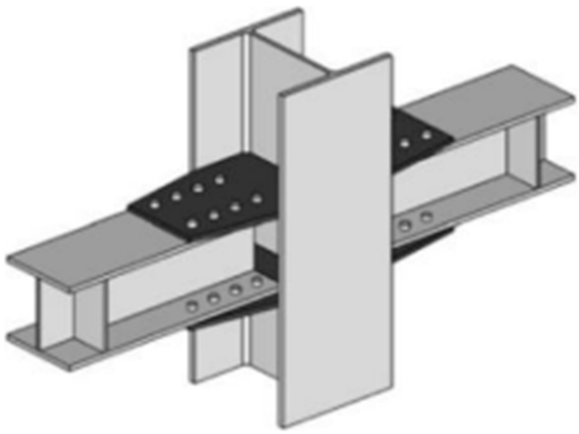

Figure 1. Connection proposed by Shim.

Kim et al. [15] illustrated a composite beam-to-column joint to explain that one of the reasons for failure is the concrete slab, which causes the neutral axis to move toward the top flange when the beam is subjected to positive beam bending (concrete slab under compression), causing the strain of the lower flange to be much greater than that of the top flange and leading to premature connection brittle failure. In addition to the issues with the concrete slab, the shear deformation of the panel zone can also harm the strain of the lower flange of the beam, leading to excessive demand for tensile strain and causing the weld to fracture between the beam's lower flange and the column. For example, Adlparvar et al. [16] studied the impact of panel zone shear strength on the seismic behavior of enhanced slotted-web beam connections, and their results indicated that high participation of the panel zone effect increased the likelihood of beam web weld fracture. Miri et al. [17] also found that in frames with weak panel zones, the story drifts are more than the permitted rate according to design standards, and the story drifts could be reduced by reinforcing the panel zone. Therefore, for an SMF with I-section columns, in a typical weak panel zone steel frame, it was necessary to provide substantial inelastic deformation capacity via flexural yielding in the beams and restricted elastic deformation in panel zones.

The steel SMF's seismic design is often based on two concepts: high ductility–low bearing capacity or low ductility–high bearing capacity. However, according to the rules of the specification GB50011-2010 [18], the seismic design of SMFs should follow high ductility–high elastic bearing capacity for strong columns and weak beams and strong joints and weak components. When SMFs fail during an earthquake, plastic hinges emerge on the beam ends, but no plastic failure occurs in the columns or panel zones. To realize this design concept, a novel type of joint must combine a strong panel zone with high ductility and bearing capacity. In 2018, Lu et al. [19] proposed a box-strengthened panel zone joint for SMFs with I-section columns, which were typical weak panel zone steel frames, as shown in Figure 2, and gave the detailed construction procedure and methods of the developed connection. It has good rotational ductility, its plastic rotation capacity is more than 0.03 rad, and its bearing capacity is slightly higher than that of the box-section column [19]. It also has strong panel zone characteristics and can effectively achieve seismic functions such as plastic hinge displacement at the beam end [19]. Thus, this study analyzes the influence of this new panel zone on the seismic performance and story drifts of steel SMFs by tests and numerical analyses to promote the engineering use of this new panel zone connection.

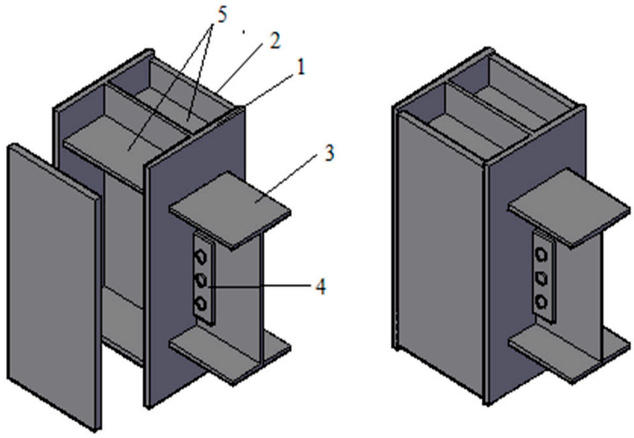

Figure 2. The box-strengthened panel zone joint. 1. I-section column; 2. Skin plate (pair); 3. H-shaped beam; 4. Shear plate; 5. Diaphragm (two pairs).

2. Design Specification for the Box-Strengthened Panel Zone Joint

In order to avoid the recurrence of the Northridge earthquake damage, it is essential to consider the combination effect of concrete slabs and propose technical measures to reduce panel zone shear deformation in the design of the post-Northridge connection. Due to the complexity of the failure mechanism of composite joints, even when some design codes adopt steel–concrete composite beams, the design of steel frame connections, considering the influence of concrete slabs, has not been included in existing specifications. On the contrary, some specifications accept strengthening SMFs' panel zones [17–19]. The two specifications, GB50011-2010 [18] and ANSI/AISC 341-22 [20], both require the seismic design of the panel zone, including the required shear strength, the panel-zone thickness, and the requirements of panel-zone doubler plates, which are used if the thickness of the column web does not meet that shown in Equation (1) [18,20].

$$t \geq (d_z + w_z)/90, \quad (1)$$

where $d_z = d - 2t_f$ of the deeper beam at the connection, d is the total depth of the beam in. (mm), and t_f is the thickness of the beam flange, in. (mm); t = thickness of column web or individual doubler plate, in. (mm); w_z = width of panel zone between column flanges, in. (mm).

When plug welds are used to join the doubler plate to the column web, the total panel-zone thickness is permitted to satisfy Equation (1). Additionally, the individual thicknesses of the column web and doubler plate shall satisfy Equation (1), where d_z and w_z are modified to be the distance between plug welds. When plug welds are required, a minimum of four plug welds shall be provided and spaced in accordance with Equation (1).

However, except in Equation (1), the limit state of shear yielding needs to be checked according to Equation (2) [18].

$$\Psi(M_{pb1} + M_{pb2})/V_P \leq (4/3)f_{yv}, \tag{2}$$

where M_{pb1}, M_{pb2} = the fully plastic bending bearing capacity of beams on both sides of the panel zone, respectively; Ψ = reduction factor; f_{yv} = shear yield strength; V_P = volume of panel zone; for the I-section column, $V_P = d_z w_z t$, and for box-section column, $V_P = 1.8 d_z w_z t$.

The volume of the panel zone of the box-section column should be double that of the I-section column, which was reduced by 10% when implemented in GB50011-2010 [18]. The author proposed the construction of the box-strengthened panel zone of the I-section column depicted in Figure 2 regarding the shape of the box-section column panel zone. The volume of the panel zone of the I-section column shown in Figure 2 is greater than that of the box-section column when the thickness of the skin plate is the same as that of the box-section column wall plate because it has an extra column web in its panel zone. Existing research has demonstrated that the stiffness of a box-strengthened panel zone joint is greater than that of the box-section panel zone joint [19].

3. Experiment Investigation on the Seismic Behavior of a Steel SMF with a Box-Strengthened Panel Zone

Of course, according to the design specifications [18,20], adding the doubler plates will also increase the volume and stiffness of the I-section column panel zone and reduce the story drifts [17]. However, the design specification GB50011-2010 requires that the calculation of an SMF's story drift when it uses I-section columns must consider the shear deformation of the panel zone, while for an SMF that uses box-section columns, it is not necessary. In frames characterized by vulnerable panel zone areas, in 2009, Miri et al. [17] observed that when story drifts exceed the permissible limits defined by design standards, reinforcing the panel zone with doubler plates can effectively mitigate the development of excessive story drifts, but the deficiency of their research is that they did not quantitatively analyze the contribution of shear deformation in the panel zone strengthened by doubler plates to the story drifts. In order to investigate the influences of shear deformation on the story drift of SMFs, an SMF specimen experiment was conducted.

3.1. Experiment Specimen

We designed a Q235 steel SMF specimen, as shown in Figure 3. The column was HW300 × 300 × 10 × 15, and the beam was HN350 × 175 × 7 × 11. The thickness of the skin plate was 16 mm, the thickness of the diaphragm was 12 mm, and the thickness of the shear plate was 8 mm. Beam top and bottom flanges and column flanges or skin plates were fully penetrated bevel butt-welded with an E4311-type welding electrode; the beam web and the connection plate welded to the column flange or skin plate were connected by six 10.9-grade M20 high-strength bolts. The mechanical properties of steel plates, welds, and H-shapes are listed in Table 1.

Table 1. Member sections and analysis results.

Item	f_y/MPa	f_u/MPa	E/MPa	δ/%
Column web, 10 mm	278.7	460.6	206 162	28.4
Column flange, 15 mm	253.1	472.1	208 780	27.1
Beam web, 7 mm	332.2	468.0	202 324	27.8
Beam flange, 11 mm	295.5	443.2	204 381	29.1
Skin plate, 16 mm	275.0	443.3	207 000	29.7
Diaphragm, 12 mm	295.0	443.2	206 130	28.9
Shear plate, 8 mm	305.5	440.4	206 600	29.3
Welds	398.3	496.7	208 000	18.8

f_y is measured yield strength; f_u is measured tensile strength; E is measured modulus of elasticity; δ is elongation ratio.

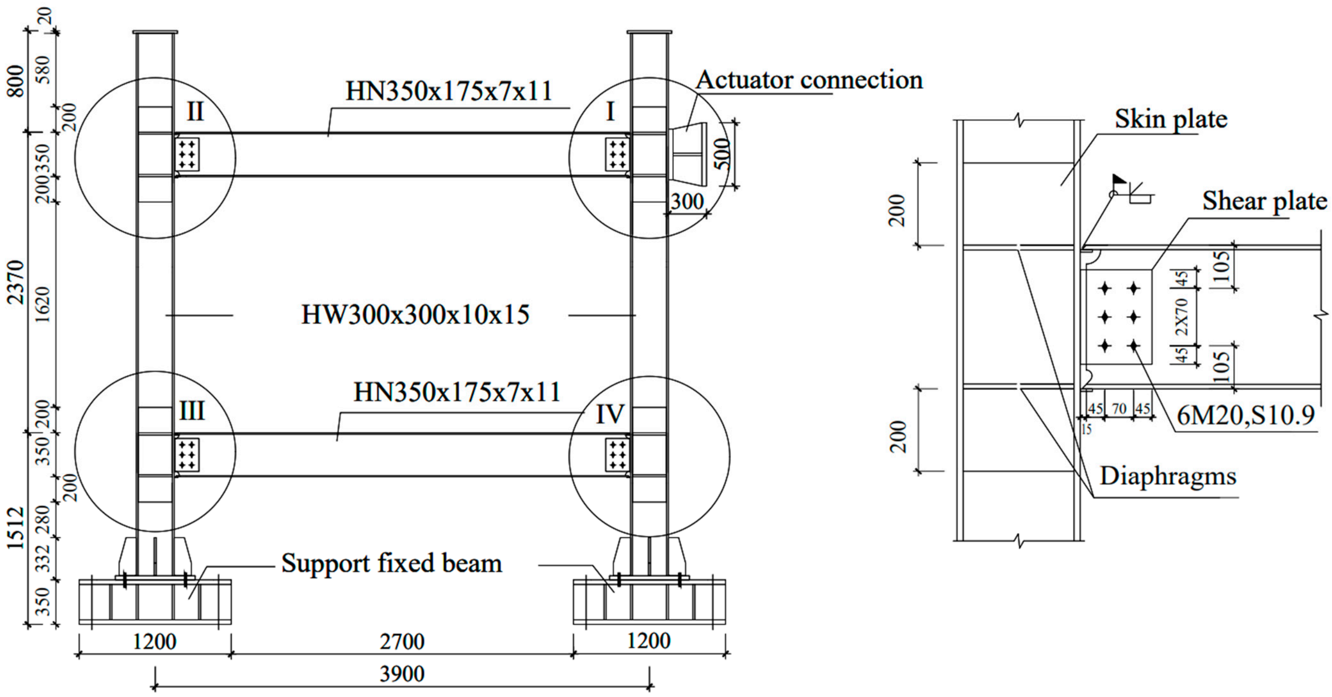

Figure 3. The box-strengthened panel zone SMF and joint details.

3.2. Loading Setup and System

Figure 4 depicts the test loading configuration. The specimen's columns were connected to the support fixed beam via a stiff exposed column base secured to the ground with a compression beam. Two anchor bolts secured the pressure beam to the base channel. Four horizontal lateral supports were installed on both sides of the beam in the first and second stories of the specimen to avoid lateral-torsional buckling and out-of-plane bending of the beam.

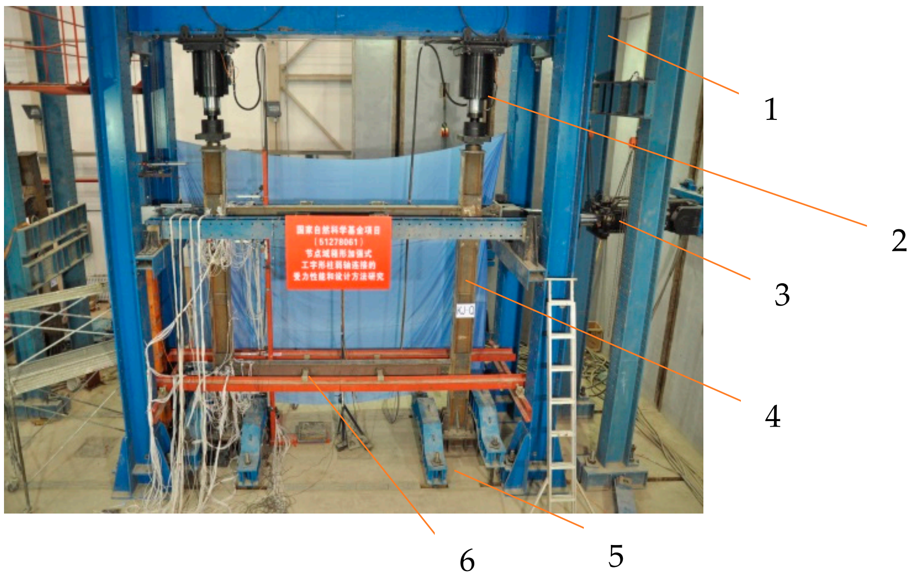

Figure 4. Test setup. 1. Loading portal steel frame; 2. Electro-hydraulic servo jack; 3. MTS actuator; 4. Steel frame specimen; 5. Compression beam; 6. Lateral support. Note on the red signboard: Nature Science Foundation of China (51278061), research on the mechanical performance and design methods of the weak axis connection of the box-strengthened panel zone of the I-section column.

An MTS actuator with a maximum thrust of 1460 kN, an ultimate tensile force of 960 kN, and a stroke of 250 mm was used for horizontal loading. An electro-hydraulic servo vertical loading gantry system with a maximum loading capacity of 3000 kN was used for vertical loading. The data were gathered using the IMP static data gathering equipment. A vertical force was applied in four stages at the top of the column based on the axial compression ratio of 0.45. After each load level was used and stabilized for three minutes, we checked whether the load value was constant and eliminated the installation gaps of the loading device and the specimen. The first stage used 286 kN, the second used 573 kN, the third used 859 kN, and the fourth used 1146 kN. The vertical force of 1146 kN remained constant throughout the test. Through finite element numerical simulation before the test, the calculated yield load displacement was confirmed as 20 mm. Therefore, after vertical loading of 1146 kN, the MTS actuator applied a low cycle repeating load corresponding to the displacement step. The loading steps are shown in Figure 5. There was a displacement of 4 mm in each direction per loading step with a loading rate of 0.5 mm/s and three cycles at each step. After the horizontal load dropped to 85% of the peak load, we continued loading for one more cycle and stopped the test.

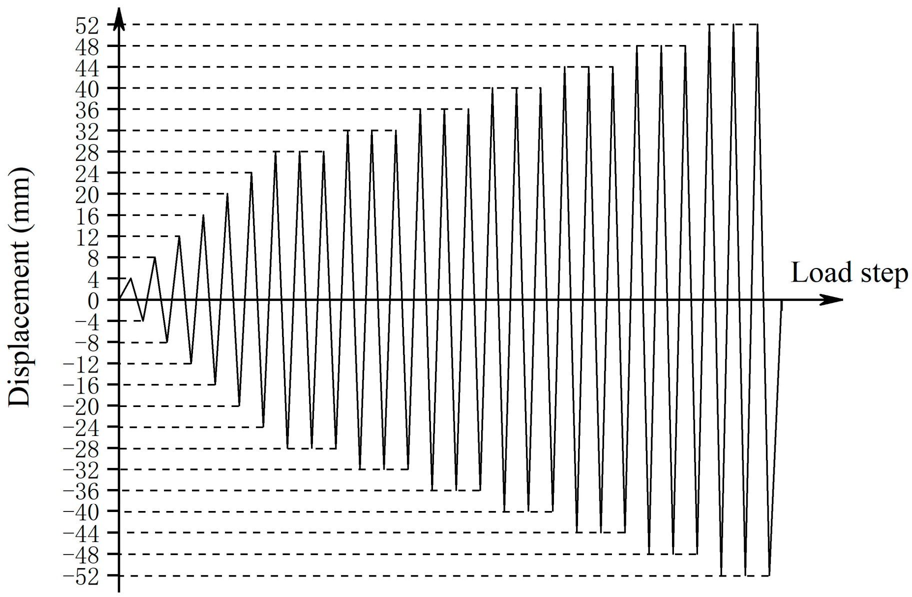

Figure 5. The loading steps.

3.3. Displacement Meter Arrangement

Figure 6 depicts the experiment's layout of displacement meters and strain gauges. D1 and D2 displacement meters detected the horizontal displacement of the beam on the second and first floors, respectively. The horizontal displacement of the top and bottom of the specimen column was measured by displacement meters D3 and D4. The horizontal movement of the support fixed beam was measured using a displacement meter D5. In order to describe the test phenomenon easily, this research divided the nodes of the frame specimen into four areas, marked with Roman numerals I, II, III, and IV, respectively, as shown in Figure 3. The rotational deformation of II and III beam-column joints was measured using displacement meters D6, D7, D8, and D9. The rotational deformation of II and III columns was measured using displacement meters D10, D11, D12, and D13, respectively. At the appropriate places, displacement meters D14, D15, and D16 were used to measure the vertical deflection of the second-story beam; displacement meters D17, D18, and D19 were used to measure the vertical deflection of the first-story beam.

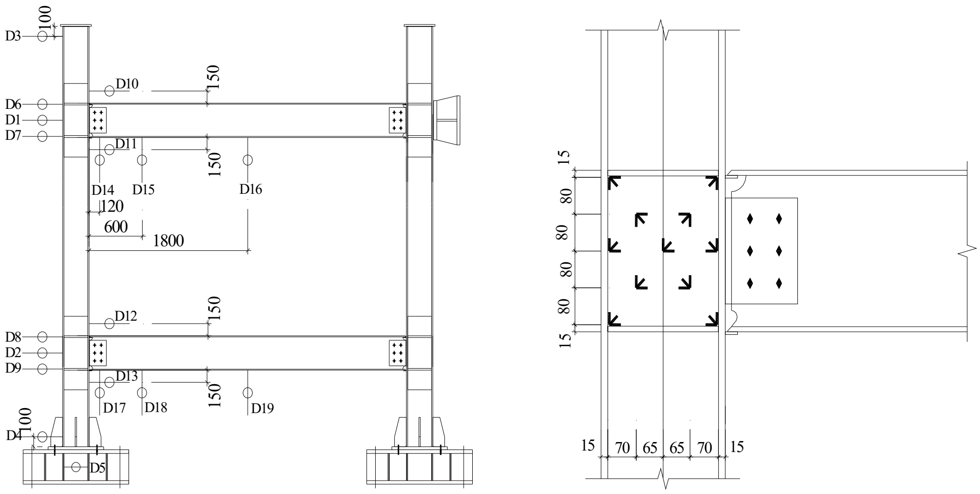

(**a**) (**b**)

Figure 6. Displacement meter and strain gauge arrangement: (**a**) displacement meters; (**b**) strain gauges.

The strain gauges were arranged in the panel zones (skin plates) of areas II and III, and a typical arrangement is shown in Figure 6b. The strain gauge measured the shear strain in the panel zone and monitored its stress state (elasticity, elastoplasticity, or plasticity) when the specimen was damaged.

3.4. Test Phenomena and Failure Characteristics

When a horizontal displacement of 28 mm was applied, the strain approached yield. The top flange of the beam end I buckled in the first cycle when loaded to 48 mm (Figure 7a), and the column base flanges buckled somewhat in the second cycle. The lower flange of the beam end II buckled when loaded to 52 mm (Figure 7b). When loaded to 56 mm, the web of the beam end I buckled in the first cycle, the upper column flange of the beam end IV buckled in the second cycle, and the middle part of the beam cracked at about 30 mm from the column flange at the lower flange of the beam end II (Figure 7c) and the upper part of the column flange III buckled in the third cycle. The lower flange at the beam end II shattered entirely after the second cycle when loaded to 60 mm. The top flange of the beam end I split when loaded to 64 mm, and the beam web bulged in an entire waveform (Figure 7d). The top flange of the beam end I entirely shattered when loaded to 68 mm, causing the specimen to fail. Figure 8a depicts the overall failure morphology, and Figure 8b shows the panel zone's stresses at the peak loading state in area II. The horizontal displacement for this peak loading condition was 56 mm.

The specimen yielded first at the upper flange of beam end I because the I joint was closer to the loading point than the others when all of the specimen's frame beams met the bending rigidity. Nonetheless, the specimen fractured sequentially at the lower flange of beam end II and the upper flange of end I, both of which were steel plate fractures. During the loading process of the test, the ball joints of the left and right column top jacks appeared to be locked, causing the force on part II of the specimen to be significantly greater than that on part I, which led to the accumulation of tensile damage and the cracking of the steel plate. The upper flange steel plate at the beam end I fractured when the tensile displacement reached 64 mm, and the failure position was roughly symmetrical with the center of the beam's lower flange failure position. This indicated that the energy released by the fracture of the lower flange of beam end II was diagonally transmitted to the upper flange of beam end I.

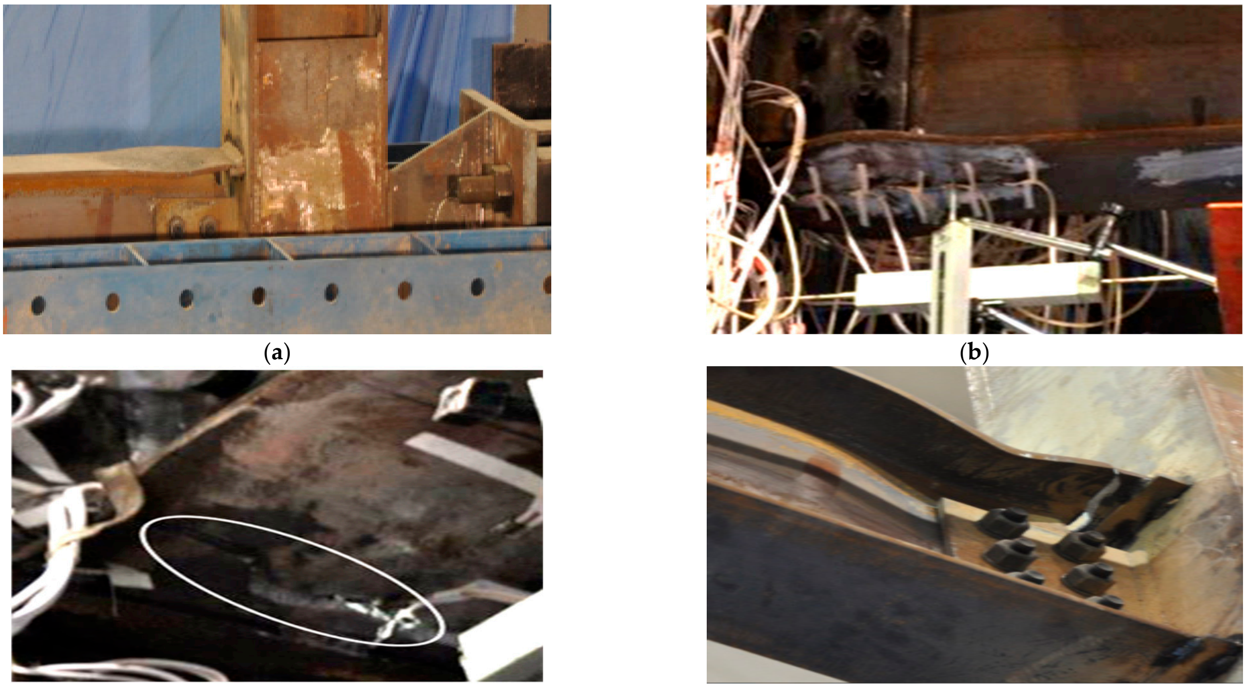

(**a**) (**b**)

(**c**) (**d**)

Figure 7. The local failures of the specimen: (**a**) the beam upper flange buckling in area I; (**b**) the beam lower flange buckling in area II; (**c**) the beam lower flange fracture in area II; (**d**) the beam upper flange fracture and web buckling in area I.

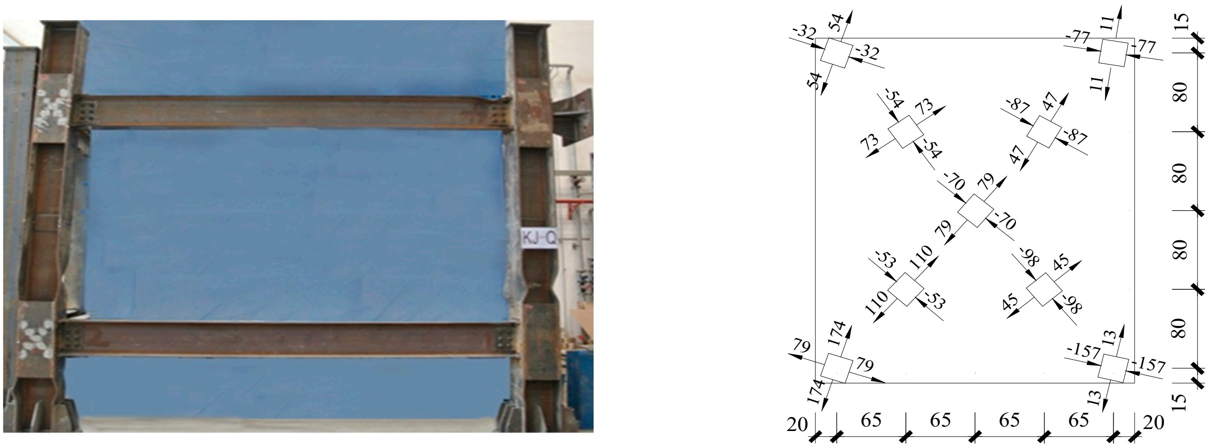

(**a**) (**b**)

Figure 8. The failure mode and panel zone stress of the specimen: (**a**) the overall failure when the horizontal loading displacement was 68 mm; (**b**) the stress of the panel zone in area II when the horizontal loading displacement was 56 mm (unit: MPa).

Figure 8b demonstrates this: (1) The stress in the panel zone was often low, indicating that the panel zone remained elastic even at peak load and did not contribute to energy dissipation. This supported the earlier conclusion that a box-strengthened panel zone is strong. (2) The stress at the panel zone measuring locations was generally distributed along the diagonal direction, with one diagonal direction in tension and the other in compression. This demonstrated that shear deformation occurs in the panel zone, although it is elastic. (3) The principal stresses were quite high at the two corners of the panel zone closest to the beam flange, and the direction deviated from the diagonal direction to some amount. This demonstrated that the tensile and compressive stresses of the beam flange butt weld had a substantial impact on the stress distribution in the panel zone.

3.5. Seismic Behavior Analysis

The specimen's hysteretic and backbone curves are shown in Figure 9. In the pictures, P denotes the actuator's load (pushing forward and pulling back), and Δ represents the inter-story displacement of the specimen. Figure 9a demonstrates that the specimen is in the elastic phase early in the experimental loading, and the hysteretic curve is almost straight. As the loading displacement rises, the hysteretic curve fills out, forming a shuttle shape. This shows that, despite the box-reinforced panel zone strengthening the frame, the frame still had a high energy dissipation capacity. Local buckling occurred at the column base flange sites of the left and right columns during the loading process, resulting in a reduction in the lateral stiffness of the specimen during the mid-term (corresponding to loading displacement in the period of 20 mm to 40 mm) of the experimental loading. The hysteretic curve revealed a pinching trend later in the experiment due to the abrupt drop in specimen stiffness produced by the consecutive fracture of the second-story beam's top and lower flange plates. According to FEMA273 [21], the specimen's yield load, maximum load, and ultimate load, as shown in Figure 9b, and their associated inter-story displacements were estimated using the backbone curve of the specimen, as given in Table 2. Table 2 shows that the specimen's reverse bearing capacity was greater than its forward bearing capacity, but its reverse displacement ductility coefficient was less than its forward displacement ductility coefficient. This is consistent with the test's observation of early fracture in the opposite direction.

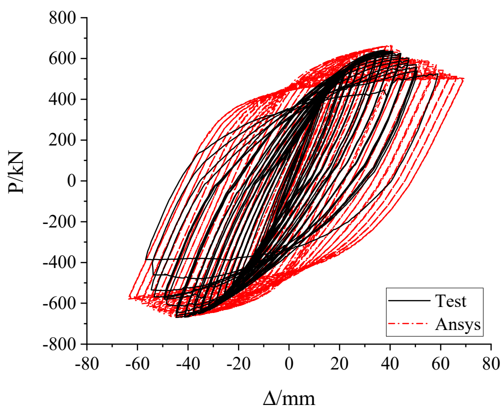

(**a**)

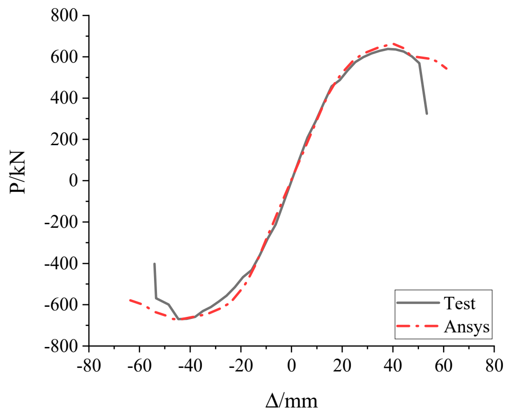

(**b**)

Figure 9. The curves of the specimen: (**a**) hysteretic curve; (**b**) backbone curve.

Table 2. Test results.

Loading Direction	P_y/kN	Δ_y/mm	P_{max}/kN	Δ_{max}/mm	P_u/kN	Δ_u/mm	Ductility Coefficient
+	481.2	18.9	638.1	37.9	542.4	55.6	2.94
−	472.7	19.9	669.7	44.7	569.2	53.4	2.68

P_y, P_{max}, and P_u represent the yield, maximum, and ultimate loads of single-bay frames, respectively. Δ_y, Δ_{max}, Δ_u is the inter-story displacement corresponding to P_y, P_{max}, P_u.

According to the relationship between the inter-story displacement angle and the inter-story displacement, $\theta = \Delta/h$, it was calculated that when the specimen reached the yield load, the corresponding inter-story displacement angle was 1/125 and was greater than 1/250; when the specimen reached the failure load, the corresponding inter-story displacement angle was 1/43 and was greater than 1/50. They all met the requirements of specification GB 50011-2010 [18].

3.6. Panel Zone Shear Deformation

Through the strain gauges arranged on the diagonal line of the panel zone, the strain value along the diagonal line of the panel zone of the specimen during the loading process was measured. The shear deformation angle of the panel zone during the test was calculated by Equation (3).

$$\gamma = \frac{\sqrt{a^2+b^2}}{ab}\overline{\mathrm{X}}, \tag{3}$$

where a is the height of the panel zone, b is the width of the panel zone, and $\overline{X}$ is the average strain value in the diagonal direction.

In comparison, the theoretical shear deformation angle was calculated by Equation (4) following the specification GB50011-2010 [18].

$$\gamma_i = \frac{1}{n}\sum\frac{M_{j,i}}{GV_{\mathrm{pe},ji}}, (j = 1, 2, \cdots n), \tag{4}$$

where $G = 7900\ \mathrm{kN/cm^2}$ is the shear elasticity modulus of Q235 steel, V_{pe} is the effective volume of the panel zone calculated by Equation (2), and $M_{j,\,i}$ is an unbalanced moment of j-th panel zone in the i-th floor.

Table 3 shows the shear deformation angle of the panel zone within the elastic stress range of the specimen. Among these values, Δ_t is the horizontal displacement imposed during the test, Δ_1 represents the approximate frame inter-story displacement without considering the shear deformation of the panel zone, which was calculated according to the real-time value of the displacement meters, Δ_2 represents the frame inter-story displacement that was accurately measured considering the shear deformation of the panel zone, and Δ_3 is the frame inter-story displacement according to GB 50011-2010 [18]. The shear deformation angle of the panel zone was calculated according to Equations (3) and (4). In Table 3, γ represents the panel zone's yield shear deformation angles calculated by Equation (3), and γ_c represents the panel zone's yield shear deformation angles calculated by Equation (4).

Table 3. Comparison of frame inter-story displacement and panel zone shear deformation.

Δ_t/mm	Δ_1/mm	Δ_2/mm	Δ_3/mm	Δ_n/mm	$\gamma/10^{-3}$ rad	$\gamma_c/10^{-3}$ rad	γ/γ_c/%
4	3.1	3.119	4.2	3.3	0.008	0.4	2
8	6.3	6.336	8.4	6.6	0.015	0.9	1.7
12	9.5	9.557	12.4	10.0	0.024	1.2	2.0
16	12.6	12.676	16.4	13.3	0.032	1.6	2.0
20	15.8	15.897	20.4	16.6	0.041	2.0	2.1
24	18.7	18.828	23.6	19.8	0.054	2.1	2.6
28	22.1	22.256	27.5	23.2	0.066	2.2	3.0

Table 3 shows that the specimen's Δ_2 was similar to the Δ_1, which is the inter-story displacement without considering the shear deformation of the panel zone, and the increase in Δ_2 over Δ_1 was only 0.6% to 0.7%, showing that the contribution of the shear deformation of the panel zone was almost equal to zero. That means the shear deformation of the box-strengthened panel zone hardly enhanced the frame's inter-story displacement. Moreover, the actual shear deformation of the panel zone γ was only 3% of the theoretical value γ_c. Therefore, the guidelines in GB 50011-2010 [18] for box column steel frames could be followed, and the effect of panel zone shear deformation on inter-story displacements was not considered. This proves that a box-strengthened panel zone is more robust than the standard panel-zone doubler plates because it can form the box-shape panel zone in SMFs that use I-section columns.

4. Numerical Analysis Validation

4.1. Numerical Model Development

Based on the test, the cyclic loading analysis of the steel frame was carried out using ANSYS 16.0. The idealized bi-linear stress–strain steel constitutive model without strength degradation was used for the model. The yield stress σ_y, the yield strain ε_y, and the ultimate tensile stress σ_u and strain ε_u were determined through the carbon steel tensile test, as shown in Table 4 [22]. The bonded contact type imposed the beam-to-column interaction. Its beam and column components, skin plate, and column diaphragms all used SOLID95 elements. Since the overall deformation of the steel frame was investigated, the bolts, welds, and component's residual stresses were ignored in the modeling.

Table 4. Steel material properties used in ANSYS.

Steel Profiles	Thickness (mm)	Young's Modulus (MPa)	True Plastic Strain	True Stress (MPa)
Column flange	15	2.02×10^5	0.0	285
			0.2	525
			0.4	553
			0.6	567
Skin plate	16		0.8	580
			1.0	592
Beam flange	11	2.04×10^5	0.0	307
			0.2	534
			0.4	572
			0.6	600
Column web	10		0.8	619
			1.0	635
Beam web	7	2.06×10^5	0.0	332
			0.2	553
			0.4	607
			0.6	647
			0.8	670
			1.0	690

In addition, the point element MASS21 element, with six degrees of freedom, was chosen for the load points. Like the testing protocol, the boundary condition at the bottom of the column was assumed to limit all degrees of freedom, which means it was fixed. The lateral bracing constraints in the Z direction (vertical paper orientation) were imposed on the position of 1000 mm distanced from beam ends (see Figure 10a). The vertical loading point at the top beam end was subjected to the lateral displacement in the X-direction, and the repeated X-direction displacement was applied at the horizontal loading point of the beam-to-column joint, as shown in Figure 10a. The FE mesh used hexahedral elements with the most regular shapes for mapping and division. The box-strengthened panel zone within the height of the skin plate and the beam ends within the influence range of the joint measured 30mm; the other parts were 50 mm.

4.2. Numerical Analysis Verification

In general, ANSYS analysis revealed that the specimen's failure mode was the plastic hinge zone created in the beam end and panel zones maintained in an elastic condition, as well as buckling of the column flange at the column foot (Figure 10b). The overall failure pattern obtained from the numerical analysis was similar to the experimental one. Since many idealized factors existed in the numerical analysis model, the hysteretic curve derived by numerical analysis, as illustrated in Figure 9a, should have been fuller than the experimental curve. However, the two agreed on the backbone curve, which was used to calculate the critical parameters. Figure 9b shows that the test and ANSYS agreed on the initial stiffness and deformation trend. The ANSYS gave a maximum positive load of

663.9 kN and a displacement of 41.1 4 mm, which were 4% and 8.5% greater than the test result of 638.1 kN (37.9 mm), respectively. ANSYS produced a maximum negative load of −670.8 kN and a displacement of −45.5 mm, which were 0.002% and 0.2% greater than the test result of −669.7 kN (44.7 mm), respectively. Table 3 shows the numerically calculated inter-story displacement, Δ_n. Its inaccuracy from experimental measurements Δ_2 ranged from 4.2% to 5.8%. In conclusion, ANSYS numerical analysis provided reasonable accuracy and reliability and may be utilized for future parameter investigations.

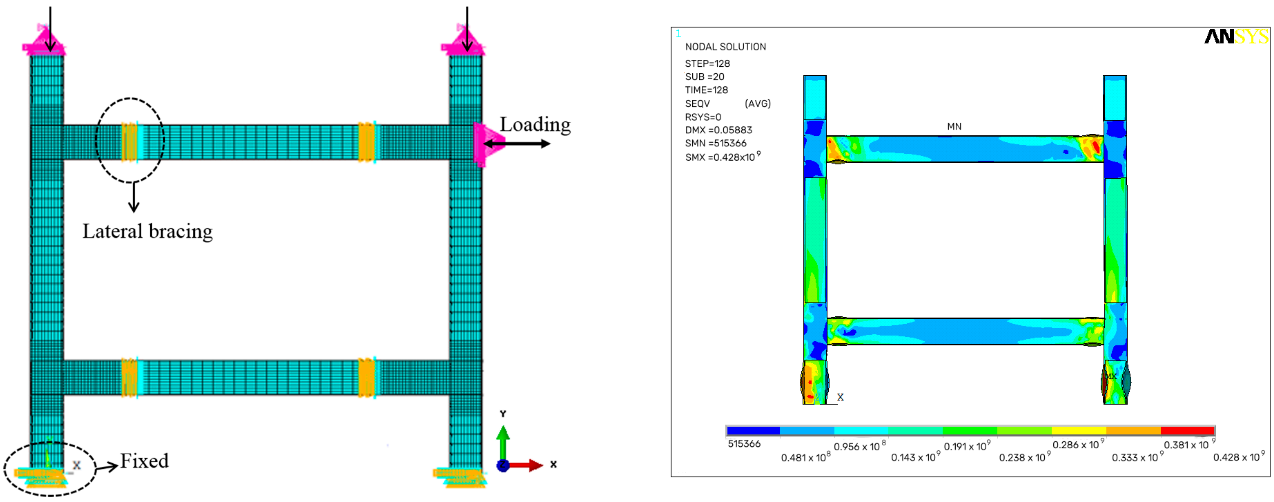

(**a**) (**b**)

Figure 10. FE analysis model and failure mode of the specimen: (**a**) FE model; (**b**) FE failure mode.

5. The Factors Influencing the Effect of Panel Zone Shear Deformation on Story Drift

There were two factors analyzed: one was the axial compression ratio (u), and the other was the beam-to-column linear stiffness ratio (sr).

5.1. The Influence of Axial Compression Ratio

For this NC series of specimens, the column, beam, steel, etc., were consistent with the specimens in the test; we only changed the axial compression ratio (u) from 0.15 to 0.75. The shear deformation angle γ of the panel zone and its proportion of Δ_s story drift under different axial compression ratios are illustrated in Figure 11. Δ_s was calculated by the following.

$$\Delta_s = \frac{\Delta_2 - \Delta_1}{\Delta_3} \times 100\%, \tag{5}$$

where Δ_1 = the approximate frame inter-story displacement without considering the shear deformation of the panel zone in. (mm), Δ_2 represents the frame inter-story displacement considering the shear deformation of the panel zone in. (mm), and Δ_3 is the frame inter-story displacement in. (mm) according to GB 50011-2010 [18].

From Figure 11a, it can be seen that the γ increased following the increase of loading displacement and axial compression ratio. However, as shown in Figure 11b, the proportion of Δ_s increased following the increase of axial compression ratio but declined following the increase of loading displacement, and the proportions of Δ_s to the story drift were from about 10% to 4%. Consequently, the box-strengthened panel zone connection reduced the development of panel zone shear deformation and brittle failure in the beam end weld zone, and the story drift increment of the steel frame did not exceed 10%. When considering the design of real SMFs, the axial compression ratio is generally strictly controlled and will not exceed 0.75. At this time, the shear deformation of the panel zone itself contributes less than 10% to the inter-story displacement. Therefore, its impact can be ignored during design when the axial compression ratio is less than 0.75.

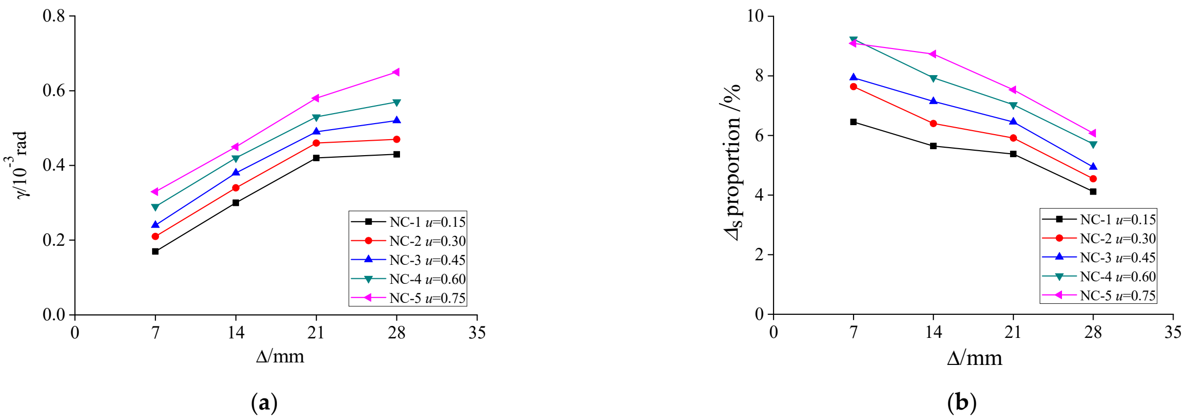

Figure 11. Shear deformation comparison of NC series of specimens: (**a**) shear deformation angle γ; (**b**) proportion of Δ_s.

5.2. The Influence of Beam-to-Column Stiffness Ratio

In the Chinese standard GB50011-2010 [18], strong columns and weak beams are provisions that must followed. The most essential condition affecting the strong columns and weak beams is the linear stiffness ratio of beams to columns. Therefore, the primary way to change sr (beam-to-column stiffness ratio) for SRC series specimens is to change the beam length (frame span). The column was HW 300 × 300 × 10 × 15, and the beam was HN 350 × 175 × 7 × 11. We changed the frame span from 3.9 m to 3.3 m, 3.0 m, 2.7 m, and 2.6 m, and the linear stiffness ratios corresponded to 0.66, 0.78, 0.858, 0.953, and 1.0.

In Figure 12a, the γ increases following the increasing loading displacement and linear stiffness ratio. However, from Figure 12b, it can be seen that the proportion of Δ_s increases following the increase of linear stiffness ratio, but the proportion of Δ_s declines following the increase of loading displacement. However, the proportions of Δ_s to the story drift were between 10% and 5%. Therefore, when the linear stiffness ratio of beam-to-columns did not exceed 1.0, the shear deformation of the panel zone itself contributed less than 10% to the inter-story displacement, and its impact can therefore be ignored during design.

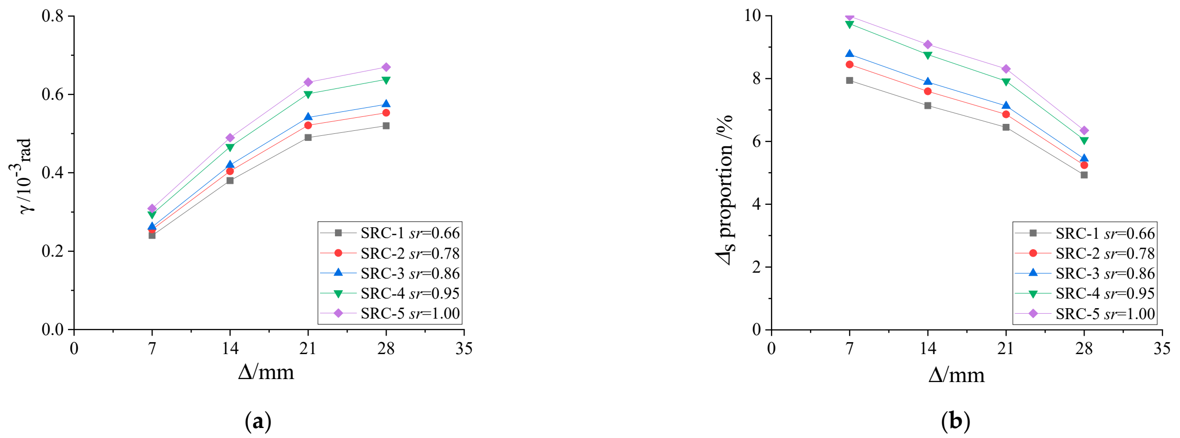

Figure 12. Shear deformation comparison of SRC series of specimens: (**a**) shear deformation angle γ; (**b**) proportion of Δ_s.

6. Conclusions

This paper investigated the influence of a box-strengthened panel zone on the seismic performance and story drift of steel SMFs by test and numerical methods. The following conclusions were obtained.

1. The seismic performance of steel frame specimens using the box-strengthened panel zone is good.

2. The box-strengthened panel zone is a type of strong panel zone. It is more robust than the standard panel-zone doubler plates and can effectively reduce the inter-story drift of steel SMFs.
3. The axial compression ratio and the beam-to-column linear stiffness ratio have the same influence on the shear deformation of the panel zone.
4. Under design conditions where the axial compression ratio is less than 0.75 and the beam-to-column linear stiffness ratio is less than 1.0, the contribution of panel zone shear deformation to the frame's inter-story drift does not exceed 10%. Its impact can be ignored during design.

Author Contributions: Conceptualization, L.L.; software, J.Z; validation, J.Z., G.Z., H.P. and B.L.; resources, L.L.; writing—original draft preparation, L.L.; writing—review and editing, L.L. and H.H.; project administration, L.L.; funding acquisition, L.L. All authors have read and agreed to the published version of the manuscript.

Funding: This research was funded by the Nature Science Foundation of China (NSFC), grant number 51278061.

Data Availability Statement: The data presented in this study are available on request from the corresponding author. The data are not publicly available due to patent protection.

Acknowledgments: The authors thank the China Scholarship Council.

Conflicts of Interest: The authors declare no conflict of interest.

References

1. León, D.D.; Reyes, A.; Yu, C. Probabilistic assessment of connections for steel buildings on seismic zones. *J. Constr. Steel Res.* **2013**, *88*, 15–20. [CrossRef]
2. Memari, M.; Mahmoud, H. Performance of steel moment resisting frames with RBS connections under fire loading. *Eng. Struct.* **2014**, *75*, 126–138. [CrossRef]
3. Wu, H.H.; Zhou, T.H.; Liao, F.F.; Lv, J. Seismic behavior of steel frames with replaceable reinforced concrete wall panels. *Steel Compos. Struct.* **2016**, *22*, 1055–1071. [CrossRef]
4. Morshedi, M.A.; Dolatshahi, K.M.; Maleki, S. Double reduced beam section connection. *J. Constr. Steel Res.* **2017**, *138*, 283–297. [CrossRef]
5. Lu, L.; Wang, D.; Ding, K.; Yan, H.; Hao, H. A Proposal for a Simple Method for Determining the Concrete SlabWidth of Composite Beam-to-Column Joints. *Appl. Sci.* **2021**, *11*, 9613. [CrossRef]
6. Koetaka, Y.; Chusilp, P.; Zhang, Z.; Ando, M.; Suitad, K.; Inoue, K.; Uno, N. Mechanical property of beam-to-column moment connection with hysteretic dampers for column weak axis. *Eng. Struct.* **2005**, *27*, 109–117. [CrossRef]
7. Cabrero, J.M.; Bayo, E. The semi-rigid behavior of three-dimensional steel beam-to-column joints subjected to proportional loading. Part I: Experimental evaluation. *J. Struct. Eng.* **2007**, *63*, 1241–1253.
8. Cabrero, J.M.; Bayo, E. The semi-rigid behavior of three-dimensional steel beam-to-column joints subjected to proportional loading. Part II: Theoretical model and validation. *J. Struct. Eng.* **2007**, *63*, 1254–1267.
9. Kim, S.D.; Kim, S.S.; Ju, Y.K. Strength evaluation of beam-column connection in the weak axis of H-shaped column. *Eng. Struct.* **2008**, *30*, 1699–1710. [CrossRef]
10. Lee, E.T.; Kang, M.J.; Kim, S.B.; Kim, S.S. Experimental study on structural performance of the new shaped weak-axis connection in full-scale test. *Int. J. Steel Struct.* **2016**, *16*, 685–696. [CrossRef]
11. Lee, K.; Li, R.; Jung, H.; Chen, L.; Oh, K. Cyclic testing of weak-axis steel moment connections. *Steel Compos. Struct.* **2013**, *15*, 507–518. [CrossRef]
12. Lee, K.; Li, R.; Jung, H.; Chen, L.; Oh, K.; Kim, K.S. Cyclic testing of steel column-tree moment connections with various beam splice lengths. *Steel Compos. Struct.* **2014**, *16*, 221–231. [CrossRef]
13. Kozlowski, A. Component method model for predicting the moment resistance, stiffness and rotation capacity of minor axis composite seat and web site plate joints. *Steel Compos. Struct.* **2016**, *20*, 469–486. [CrossRef]
14. Shim, H.J.; Lee, E.T.; Kim, S.B.; Kim, S.S. Development and performance evaluation of weak-axis column bending connections for advanced constructability. *Int. J. Steel Struct.* **2014**, *14*, 369–380. [CrossRef]
15. Kim, Y.J.; Oh, S.H.; Moon, T.S. Seismic behavior and retrofit of steel moment connections considering slab effects. *Eng. Struct.* **2004**, *26*, 1993–2005. [CrossRef]
16. Adlparvar, M.R.; Vetr, M.G.; Ghaffari, F. The importance of panel zone shear strength on seismic behavior of improved slotted-web beam connections. *J. Struct. Eng.* **2017**, *17*, 307–318. [CrossRef]
17. Mahmoud, M.; Morteza, N.; Amir, K. Panel zone rigidity effects on special steel moment-resisting frames according to the performance based design. *World Acad. Sci. Eng. Technol.* **2009**, *50*, 925–931.

18. *GB50011-2010*; Code for Seismic Design of Buildings. China Architecture & Building Press: Beijing, China, 2010.
19. Lu, L.F.; Xu, Y.L.; Lim, J.B.P. Mechanical performance of a new I-section weak-axis column bending connection. *Steel Compos. Struct* **2018**, *26*, 31–44.
20. *ANSI/AISC 341-22*; Seismic Provisions for Structural Steel Buildings. American Institute of Steel Construction: Chicago, IL, USA, 2022.
21. FEMA 273 NEHRP. *Commentary on the Guidelines for the Seismic Rehabilitation of Buildings*; Federal Emergency Management Agency: Washington, DC, USA, 1997.
22. Lu, L.F.; Xu, Y.L.; Zheng, H. Investigation of composite action on seismic performance of weak-axis column bending connections. *J. Constr. Steel Res.* **2017**, *128*, 286–300. [CrossRef]